ELSEVIER

Contents lists available at ScienceDirect

Acta Biomaterialia

journal homepage: www.elsevier.com/locate/actbio



Full length article

In vitro and in vivo studies to evaluate the feasibility of Zn-0.1Li and Zn-0.8Mg application in the uterine cavity microenvironment compared to pure zinc



Guo Bao^{a,#}, Qianqian Fan^{a,b,#}, Dongfeng Ge^{a,b}, Kun Wang^{a,b}, Mingming Sun^{a,b}, Zechuan Zhang^c, Hui Guo^c, Hongtao Yang^c, Bin He^{a,**}, Yufeng Zheng^{b,c,d,*}

- ^a Department of Reproduction and Physiology, National Research Institute for Family Planning, Beijing 100081, China
- ^b Graduate School of Peking Union Medical College, Beijing 100730, China
- ^c Department of Materials Science and Engineering, College of Engineering, Peking University, Beijing 100871, China
- d International Research Organization for Advanced Science and Technology, Kumamoto University, 2–39–1 Kurokami, Chuo-Ku, Kumamoto 860–8555, Japan

ARTICLE INFO

Article history: Received 1 August 2020 Revised 21 December 2020 Accepted 31 December 2020 Available online 16 January 2021

Keywords:
Biomedical Zn alloys
Simulated uterine fluid
In vitro
In vivo
Uterine cavity microenvironment

ABSTRACT

Significant advances have been achieved in the research evaluating Zn and its alloys as degradable metallic biomaterials mainly for application in bone and blood vessels. In the present study, the degradation behaviors of Zn-0.1Li and Zn-0.8Mg alloys in simulated uterine fluid (SUF) were systematically investigated for 300 days. *In vitro* viability assays were conducted in different uterine cells (HUSMCs, HEECs, and HESCs), and histological examination after the *in vivo* implantation into the uterine cavity was performed using pure Zn as control. The immersion test results indicated that both Zn-0.1Li and Zn-0.8Mg alloys exhibited better corrosion resistance than pure Zn, with $Zn_3(PO_4)_2 \cdot 4H_2O$ and $Zn_2(PO_4)_2 \cdot 2H_2O$ being the main corrosion products detected in the SUF in addition to ZnO. The cell cytotoxicity assays revealed that Zn-0.1Li and Zn-0.8Mg exhibited better cytocompatibility than Zn. Moreover, the *in vivo* experiments demonstrated that the Zn-0.1Li and Zn-0.8Mg alloys induced less inflammation in the uterine tissue than pure Zn, with Zn_2O and Zn_2O being the major biocorrosion products in addition to ZnO. According to these results, zinc alloys appear to be suitable potential candidate materials for future intrauterine biomedical devices.

Statement of significance

Significant advances have been made in the research on Zn and its alloys as degradable metallic biomaterials, mainly for use within bone and blood vessels. In the present study, the biodegradation behaviors of pure Zn, Zn-0.1Li, and Zn-0.8Mg alloys in simulated uterine fluid were systematically investigated, followed by the examination of cytotoxicity using three different types of cells, and the *in vivo* biocompatibility was evaluated by implanting rod samples into microenvironments of the rat uterine cavity. The better results obtained for Zn-0.1Li and Zn-0.8Mg alloys *in vitro* and *in vivo* tests indicated that it is feasible to use these alloys in future intrauterine biomedical devices.

© 2021 Acta Materialia Inc. Published by Elsevier Ltd. All rights reserved.

* Corresponding author at: Department of Materials Science and Engineering, College of Engineering, Peking University, No.5 Yi-He-Yuan Road, Hai-Dian District, Beijing 100871, China.

E-mail addresses: hebin@nrifp.org.cn (B. He), yfzheng@pku.edu.cn (Y. Zheng).

Guo Bao and Qianqian Fan contributed equally to this study.

1. Introduction

Zinc is one of the most important essential elements for the human body [1] as it is involved in a multitude of biological processes in the body [2], including nucleic acid metabolism, signal transduction, apoptosis regulation, gene expression, and protein synthesis. Zinc performs important functions in the immune [3], nervous [4], and reproductive [5,6] systems. Moreover, zinc influences the processes of tissue repair and wound healing [6] and

^{**} Corresponding author.

exhibits antibacterial and anti-inflammatory effects [7,8]. Zinc also serves as the cofactor of over 300 enzymes and participates in the structure and function of the enzyme molecules as well as in the regulation of enzyme activities [2].

Recently, extensive research has been conducted on the use of zinc and its alloys as biodegradable metals, and they have been reported to have appropriate degradation behavior as compared to magnesium and iron [9,10]. The previous targeted applications thus far have focused mainly on the use of zinc and its alloys in bone and blood vessel microenvironments. Simulated fluids such as simulated body fluid (SBF), modified simulated body fluid (m-SBF) [11], Hank's saline solution [12], and Ringer's solution [13] were used as media in the immersion tests in previous studies, and cell compatibility was evaluated using various cell lines, including certain vascular and bone-related cells such as mouse osteoblastic cells (MC3T3) [12,14,15], human bone marrow mesenchymal stem cells [16], human vascular endothelial cells [17], and human aortic smooth muscle cells [18]. Shearier et al. [19] reported that zinc ions exhibit different cell survival reduced to 50% (LD₅₀) dosages independent of the cell type used. The reported LD₅₀ concentrations of human aortic endothelial cells (HAEC), human aortic smooth muscle cells (AoSMC), and human dermal fibroblasts (hDF) were 50 μM, 70 μM, and 265 μM, respectively. Another study evaluating the effect of zinc ions on the human coronary artery endothelial cells (HCAECs) reported a biphasic effect, with the zinc ions causing increased cell viabilities at the concentration of 20 μM, while an inhibiting effect on cell viabilities was observed at 100 µM concentration of Zn ions [17].

The intrauterine microenvironment plays a critical role in the reproductive health of women [20]. An intrauterine implantable biomedical device should be designed after considering the interaction between the implanted materials and the uterine cavity microenvironment, as in the case of previously reported examples such as copper-intrauterine device (Cu-IUD) [21,22] and treatment with intrauterine adhesion (IUA) [23] of balloon and inert physical-barrier materials. In a recent study by our research group, the application of biodegradable magnesium alloys in the uterine microenvironment was investigated for the first time, and good biocompatibilities were reported [24]. Inspired by this, the present study was aimed to evaluate the *in vitro* and *in vivo* biocompatibilities of zinc and its alloys in the intrauterine microenvironment. Zn-Mg and Zn-Li alloys were selected as the experimental materials due to the following reasons:

- (1) Compared to pure zinc, the Zn-Mg binary alloys exhibit superior mechanical properties while maintaining high levels of biosafety. The extract of Zn-0.8Mg alloys contains Zn²⁺ ions at the concentration of 70 μmol/L, which presents good viabilities of 80% [25]. Moreover, the findings of our previous work indicated that the extruded Zn-1Mg alloy extracts showed extremely good viabilities in ECV304, VSCM, and MG63 cells, and the Zn-1Mg alloy rod implanted in mouse femora exhibited no negative biological effects [26].
- (2) Lithium is used widely in zinc alloys. In addition, the element Li is reported to be beneficial in the treatment of brain injury, stroke, Alzheimer's disease, Huntington's disease, and Parkinson's disease [27]. In a recent study, Zn-0.1Li alloy wire implanted into the abdominal aorta of rats exhibited excellent biocompatibility in the arterial environment [28].

In our previous study on zinc alloy implantations in orthopedics, Zn-0.1Li and Zn-0.8Mg exhibited improvements in the effective strengthening and cytocompatibility compared to zinc [29]. In the present work, a long-term *in vitro* study was performed to investigate the biodegradation behaviors of Zn-0.8Mg and Zn-0.1Li alloys in simulated uterine fluid (SUF). In addition, the *in vivo* biocompatibility was evaluated by implanting the alloys in murine

uterine cavities. The *in vitro* and *in vivo* studies evaluated the feasibility of the Zn alloys as potential candidate materials for intrauterine medical devices as compared to pure zinc (control).

2. Experimental details

2.1. Material preparation

Zinc (99.99%) and its two alloys Zn-0.1Li and Zn-0.8Mg (weight percentage, wt.%) were prepared at the Hunan Rare-Earth Material Research Institute. All the experimental material ingots were homogenized at 350 °C for 48 h, followed by water quenching and subsequent maintenance at 260 °C for 2 h prior to extrusion. The extrusion was performed with a reduction ratio of 36 at a squeeze speed of 1 mm/s. All the *in vitro* experimental discs were excised from the extruded rods, with 10 mm diameter and 2 mm thickness, followed by polishing with silicon carbide abrasive papers (SiC paper, Beijing Dongxin Grinding Tools Co., Ltd., China) with granulations from 800 to 2000 grit. The discs were cleaned ultrasonically in ethanol (Beijing Chemical works, China) for 15 min and then air-dried.

2.2. Immersion tests

The immersion tests were performed according to ASTM-G31-72 [30] in the SUF solution [NaCl 4.97 g/L, KCl 0.224 g/L, CaCl₂ 0.167 g/L, NaHCO₃ 0.25 g/L, glucose 0.50 g/L, and NaH₂PO₄ \cdot 2H₂O 0.072 g/L] (Beijing Chemical works, China) in a 37 °C water bath (Tianjin City TAISITE Instrument Co. Ltd., China), with an exposure ratio of 20 mL/cm². The tests continued for 300 days. The exposed area of the sample was approximately 2.2 cm². The SUF solution was refreshed every day from Day 1 to Day 10, every five days from Day 11 to Day 60, and finally every 30 days from Day 61 to Day 300. The change in the pH of the samples and the dissolution of zinc elements in the retrieved SUF solution were monitored and measured at the time points of SUF solution replacement. After day 1, 10, 30, 60, 150, and 300 days, five samples were retrieved from the solution, followed by gentle rinsing with distilled water and then air-drying. Subsequently, the corrosion products on the surface of the experimental samples were removed using chromic acid $(200 \text{ g/L CrO}_3 + 10 \text{ g/L AgNO}_3)$ (Beijing Chemical works, China) for 5 min at room environment. The degradation rate was determined by the following equation:

$$C = \frac{\Delta m}{\rho \times A \times t}$$

where C denotes the corrosion rate in mm/year, Δm denotes the reduction in weight, ρ denotes the density of the material, A denotes the initial surface area of the disc, and t denotes the immersion time. At least four measurements were performed for each group.

2.3. Surface characterization

The surface characteristics of the experimental samples were observed under a scanning electron microscope (SEM) coupled with an energy dispersive spectrometer (EDS) (S-4800 emission scanning electron microscope, Hitachi). The constituent phases of the corrosion product layers were identified through X-ray diffraction analysis (XRD, Rigaku DMAX 2400) using Cu-K α radiation performed at a scan rate of 4°/min, 40 kV, and 100 mA, after the samples had been immersed for respective durations. The corresponding chemical species were identified from the XRD results through peak matching analysis using MDI Jade6 software.

2.4. Electrochemical tests

The electrochemical behaviors of pure zinc, Zn-0.1Li, and Zn-0.8Mg in the SUF at room temperature were analyzed using an electrochemical workstation (Autolab, Metrohm, Switzerland). A three-electrode cell comprising a saturated calomel electrode (SCE, Tianjin Aida Hengyu Technology Development Co., Ltd., China) as the reference electrode, a platinum counter electrode (Shang Hai Ruosull Technology Co., Ltd., China), and a working electrode was employed. The exposed area of the specimen in the working electrode was 0.2826 cm². The stability open circuit potential (OCP) of each specimen was monitored for 1 h. The electrochemical impedance spectroscopy (EIS) measurement was performed by applying 10 mV perturbation, with the measuring frequency ranging from 10^5 to 10^{-2} Hz. The potentiodynamic polarization (PDP) tests were performed at the scanning rate of 1 mV/s. The corrosion parameters, including the open-circuit potential (OCP), corrosion potential (E_{corr}), and corrosion current density (i_{corr}), were analyzed through linear fit and Tafel extrapolation to the cathodic and anodic parts of the polarization curves. All the measurements were performed at least three times to verify the reproducibility of the results.

2.5. In vitro studies

2.5.1. Cells and culture

Three types of human uterine cells, namely, human uterine smooth muscle cells (HUSMC), human endometrial epithelial cells (HEEC), and human endometrial stromal cells (HESC), were used in the present study. These cells were obtained from Shenzhen Procell Company, China. The item numbers of the three primary cell types, selected and prepared through collagenase digestion and the tissue patch method, were CP-H208 for HESC, CP-H058 for HEEC, and CP-H053 for HUSMC. The preparation methods for the three cells are described below.

The uterine tissue was thoroughly washed multiple times with the phosphate-buffered solution (PBS) containing 100 U·mL $^{-1}$ penicillin and 100 g·mL $^{-1}$ streptomycin (Gibco, USA), followed by scraping inside and outside using a surgical knife to remove the mucous membrane layer and the slurry film layer. Subsequently, the muscle tissue was excised into 1 mm 3 pieces, which were then washed with the PBS containing 100 U·mL $^{-1}$ penicillin and 100 g·mL $^{-1}$ streptomycin. These washed 1 mm 3 pieces of muscle tissue were incubated in 0.15 mg·mL $^{-1}$ Collagenase II (Sigma, USA) at 37 °C for 45 min. After gently blowing into the liquid using a straw, the turbid digestive fluid was filtered by centrifugation at 300 g for 5 min. The clear portion was retained and subjected to further centrifugation at 200 g, following which the clear portion was discarded and the precipitated cells were retained.

The uterine tissue was thoroughly washed multiple times with the PBS containing $100~\rm U\cdot mL^{-1}$ penicillin and $100~\rm g\cdot mL^{-1}$ streptomycin, following which the surface mucus was scraped off and the endometrial tissue was separated. Subsequently, the endometrial tissue was incubated in 0.15 mg·mL⁻¹ Collagenase I and 1.0 U•mL⁻¹ (Sigma, USA) at 37 °C for 40 min. After adding a complete culture to terminate digestion, the endometrial surface was repeatedly scraped using a scalpel to release the epithelial cells, followed by repeatedly blowing the digestive fluid with a straw. The digestive fluid was filtered using a 200-eye cell strainer (Wuxi NEST Biotechnology Co., Ltd., China), followed by centrifugation at 300 g for 5 min. The supernatant was discarded, and the precipitated cells were retained.

The uterine tissue was thoroughly washed multiple times with the PBS containing $100~\rm U\cdot mL^{-1}$ penicillin and $100~\rm g\cdot mL^{-1}$ streptomycin; the surface mucus was then scraped off, and the endometrial tissue was separated. Subsequently, the endometrial tis-

sue was incubated in 0.15 mg·mL⁻¹ Collagenase I and 0.1 mg·mL⁻¹ trypsin (PB180225 Procell, China) at 37 °C for 40 min. After adding a complete culture to terminate digestion, the digestive fluid was repeatedly blown into by using a straw, followed by centrifugation at 300 g for 5 min; the resulting clear liquid was discarded, and the cell precipitate was retained.

The cells were characterized by immunofluorescence as described previously [24], and the images of the cell immunofluorescence are shown in Fig. S1. In the experiments, the HUSMCs were cultured in Dulbecco's Modified Eagle Medium (DMEM, Gibco, USA), while the HEECs and HESCs were cultured in DMEM: Nutrient Mixture F-12 (DMEM/F12, Gibco, USA. Both types of media contained 10% fetal bovine serum (FBS, Gibco, Origin: Australia) supplementation, $100~\text{U}\cdot\text{mL}^{-1}$ penicillin, and $100~\text{g}\cdot\text{mL}^{-1}$ streptomycin. The cultures were then incubated at 37 °C in a humidified atmosphere (HCP246, Memmert, Germany) with 5% CO₂.

2.5.2. CCK8 assay

The polished experimental samples were washed, air-dried, and then sterilized by exposing them to ultraviolet radiation for at least 4 h. The extracts were prepared by incubating the samples in either DMEM or DMEM/F12 medium supplemented with 10% FBS for 24 h at an extraction ratio of 1.25 cm²/mL under standard cell culture conditions, and the supernatant was withdrawn and stored at 4 °C until use. The pH of the extracts was measured using a pH meter (PB-10, Sartorius). The ion concentration in the extracts was determined using an inductively coupled plasma optical emission spectroscope (ICP-OES, iCAP6300, Thermo). The conventional medium was used as the negative control, and the culture medium containing 10% dimethyl sulfoxide (DMSO, Sigma-Aldrich, USA) served as the positive control.

The cells were seeded in 96-well plates at the density of 1×10^4 cell/mL (Corning2599, USA), followed by 24 h of incubation to allow attachment. Subsequently, the complete culture medium was replaced with 100% extracts, and then at Days 1, 3, and 5, prior to the test, the extracts were replaced with normal culture medium again to prevent interference. Cell viabilities were determined using the cell-counting kit-8 (CCK-8, Dojindo Molecular Technologies, Japan). Ten microliters of the CCK-8 solution was added to each well in the plate, followed by 1 h of incubation. The spectrophotometric absorbance in each well was measured using a microplate reader (Bio-RAD 680, USA) at 450 nm. Each test was repeated five times.

2.6. In vivo studies

2.6.1. Animal treatment

Sexually mature female SD (Sprague-Dawley) rats [weight range: 190-220 g; age: 8-9 weeks] were procured from the Charles River Laboratories, China. The animals were allowed to acclimatize for one week prior to conducting the experiments and were bred under standard conditions. Drinking water and conventional feed were provided ad libitum. The protocols for animal care and treatment were approved by the Ethics Committee of the National Research Institute for Family Planning (Approval No. NRIFH200408-1-3). A total of 36 sexually mature female SD rats were divided randomly into four groups depending on the implanted materials, namely the sham operation group (control group), the Zn group, the Zn-0.1Li group, and the Zn-0.8Mg group, with each group containing nine rats. Zn, Zn-0.1Li, and Zn-0.8Mg rods, each 2 mm in diameter and 10 mm in length, were prepared. The animals were anesthetized, and the corresponding material was implanted into their uterine cavity.

2.6.2. Histological analysis

The uterine tissues were collected on Days 3, 7, 14, and 28 post-implantation. The obtained uterine tissue samples were excised into small pieces of 4 mm in height, which were immediately fixed in 4% (w/v) paraformaldehyde (Sigma-Aldrich, USA) (pH 7.2) with overnight incubation at 4 °C, followed by transformation into a serial ethanol gradient (70%, 75%, 80%, 95% I and II, and 100% I and II) and then immersion in xylene and paraffin. Subsequently, 5-µm-thick uterine tissue sections prepared through microtomy (RM2235, LEICA) were dewaxed in xylene, rehydrated using decreasing concentrations of ethanol (100% I and II, 95% I and II, 80%, 75%, and 70%), and washed with phosphate-buffered saline (PBS). The sections were stained with hematoxylin and eosin (H&E) and then dehydrated using increasing concentrations of ethanol (75%, 95% I and II, and 100% I and II) and xylene. For immunohistochemistry, the sections were treated with sodium citrate antigen repair solution (ZSGB-BIO Co., Ltd. pH 6.0, 0.01 mM) for antigen repair under 90 °C bathing for 20 min. A quantity of 3% H₂O₂ was added to the sections at room temperature for 10 min. After washing thrice with PBS, the sections were blocked with normal goat serum (ZSGB-BIO Co., Ltd.) for 20 min. Subsequently, the sealant was removed from the sections, and the sections were incubated overnight at 4 °Crabbit anti-CD45 (Beijing Biodragon Immunotechnologies Co., Ltd., 1:100). After washing with PBS, the anti-rabbit secondary antibody (Beijing Biodragon Immunotechnologies Co., Ltd., 1:100) was incubated at room temperature for 1 h. After washing three times with PBS, the sections were stained with 3,3'diaminobenzidine tetrahydrochloride (DAB, ZSGB-BIO Co., Ltd.) for 5 min. Finally, the sections were re-dyed, dehydrated, and sealed. At each time point, at least 5 sections per staining in each group were subjected to tissue histological analysis. The stained specimens were examined and photographed using a high-quality microscope (Olympus CKX41, Olympus Co. Ltd., Tokyo, Japan).

2.7. Statistical analysis

All the data are presented as mean \pm standard deviation (SD). The statistical significance of these data was estimated by one-way analysis of variance (ANOVA) for multiple comparisons, followed by post-hoc SNK-q and Dunnett-t multiple comparison tests. Unless otherwise stated, the significance threshold was P = 0.05.

3. Results

3.1. Immersion in SUF

The variation in the measured pH values of the SUF throughout the immersion period for the Zn, Zn-0.1Li, and Zn-0.8Mg groups is presented in Fig. 1. The aforementioned three groups showed a rapid increase in the pH value at Day 2 of immersion, followed by a sharp decline until Day 5 and a slow upward trend afterward. Obvious differences were observed among the Zn, Zn-0.1Li, and Zn-0.8Mg groups after 180 days, at which point the pH values for the two zinc alloys were higher than that for pure zinc. The surface morphologies for the Zn, Zn-0.1Li, and Zn-0.8Mg groups exposed to the SUF solution were observed using an optical microscope after 1, 10, 30, 60, 150, and 300 days of immersion, and the results are depicted in Fig. 2a. The outputs were well consistent with the variation in the corrosion rate (Fig. 2b) at the different time points calculated through the weight loss method. The initial (Day 1) corrosion rates for the three groups were significantly higher, indicating "not substantially different" corrosion rate for each of the three alloys for an exposure period of 10 days and greater. Fig. 3 presents the release rates of zinc ions from Zn, Zn-0.1Li, and Zn-0.8Mg in the SUF over a period of 300 days. The three ion-release curves revealed that the release of zinc ions was quite high on the first

Table 1Results of the EDS analysis for pure Zn, Zn-0.1Li, and Zn-0.8Mg in the SUF (%).

		Zn	0	P	Ca
Zn	Day 1	81.42	18.58		
	Day 10	65.87	34.13		
	Day 30	24.53	65.42	8.22	1.83
	Day 60	20.39	67.12	8.45	4.03
	Day 150	19.5	59.2	14.2	7.1
	Day 300	28.02	62.25	7.82	1.9
Zn-0.1Li	Day 1	83.7	16.3		
	Day 10	30.75	62.45	6.11	0.69
	Day 30	36.46	56.06	5.46	2.03
	Day 60	22.4	55.7	10.1	2.4
	Day 150	19.26	69.04	9.16	2.54
	Day 300	19.31	65.8	11.19	3.7
Zn-0.8Mg	Day 1	82	18		
	Day 10	71.43	28.44	0.13	
	Day 30	50.66	46.52	2.44	0.39
	Day 60	50.92	48.83	0.25	
	Day 150	26.5	58.1	12.5	2.9
	Day 300	34.93	56.17	6.51	2.4

day of immersion, following which it remained relatively constant, within the limits of experimental error, for an exposure period of 10 days and greater.

3.2. Surface characterization

The surface morphologies for the three experimental groups after immersion in the SUF for 300 days are depicted in Fig. 4. After 10 days of immersion, local pitting could be observed on the surface in the Zn group, which became obvious after 30 days of immersion. With an increase in the immersion duration, the layer of corrosion products on the surface of pure zinc became thicker and further apparent. Significantly less corrosion was observed in the two zinc alloy groups compared to the pure zinc group, with only minor corrosion products detected until 60 days of immersion in the SUF. As the immersion time was extended to 300 days, the corrosion layer on the surface in the Zn, Zn-0.1Li, and Zn-0.8Mg groups became thicker, with the deposits exhibiting broccoli-like surface morphologies with lamellae or needles. The EDS results revealed the presence of Zn, O, P, and Ca elements in the corrosion products.

As presented in Table 1 and Fig. S2, the corrosion product layer observed in the three experimental groups after Day 1 mainly comprised Zn and O elements. With an increase in the immersion time, besides Zn and O, the elements P and Ca could also be detected in the surface constitution of the corrosion products. The contents of Zn were observed to gradually decrease, while the contents of O, P, and Ca increased. Moreover, as illustrated in Fig. 5, the Mg₂Zn₁₁ phase could be detected on Day 1, and the presence of this second phase continued to exist even after 150 days of immersion in the Zn-0.8Mg group. The XRD results revealed ZnO to be the main corrosion product for all three experimental materials. The corrosion product Zn₃(PO₄)₂·4H₂O was observed to be formed at the beginning of the immersion period, while CaZn₂(PO₄)₂·2H₂O was formed at the later time points during immersion (for instance, at Day 300).

3.3. Electrochemical measurements

Fig. 6 presents the potentiodynamic polarization test results for the three experimental groups in the SUF, and the obtained typical parameters are listed in Table 2. The pure Zn group showed a lower corrosion potential than the Zn alloy groups. The corrosion current density and the corrosion rate in the pure Zn group were significantly higher than those in the zinc alloy groups, although

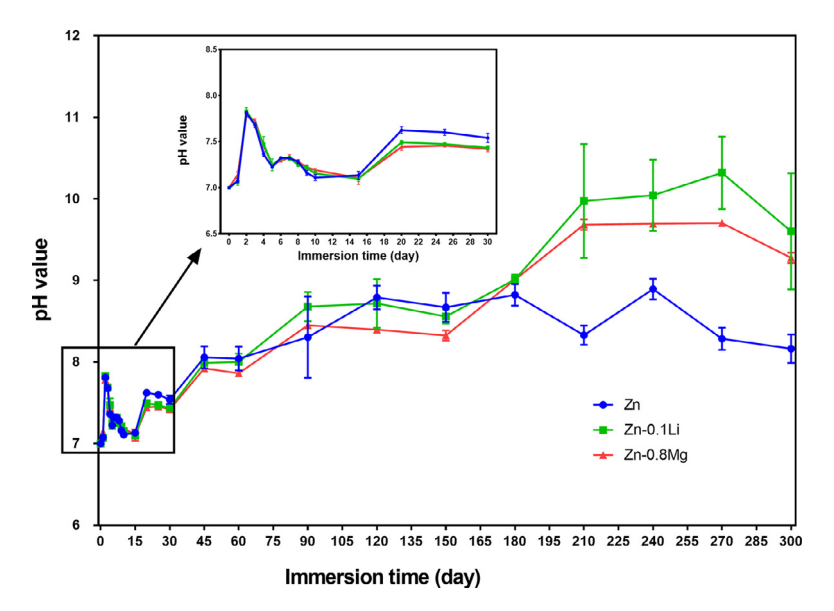


Fig. 1. Variation in pH during immersion in the SUF for 300 days for Zn, Zn-0.1Li, and Zn-0.8Mg. The line chart represents mean \pm SD; n=4.

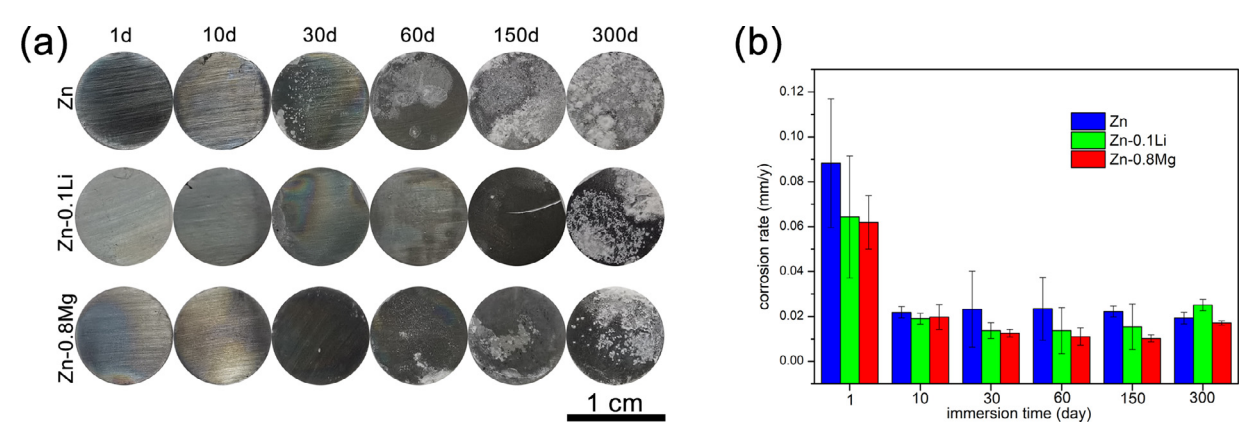


Fig. 2. (a) Surface morphologies of Zn, Zn-0.1Li, and Zn-0.8Mg exposed to the SUF solution after 1, 10, 30, 60, 150, and 300 days of immersion. (b) Corrosion rates calculated from the weight loss in the experimental samples after immersion for 1, 10, 30, 60, 150, and 300 days. The bar graph represents mean \pm SD; n = 4; *P < 0.05.

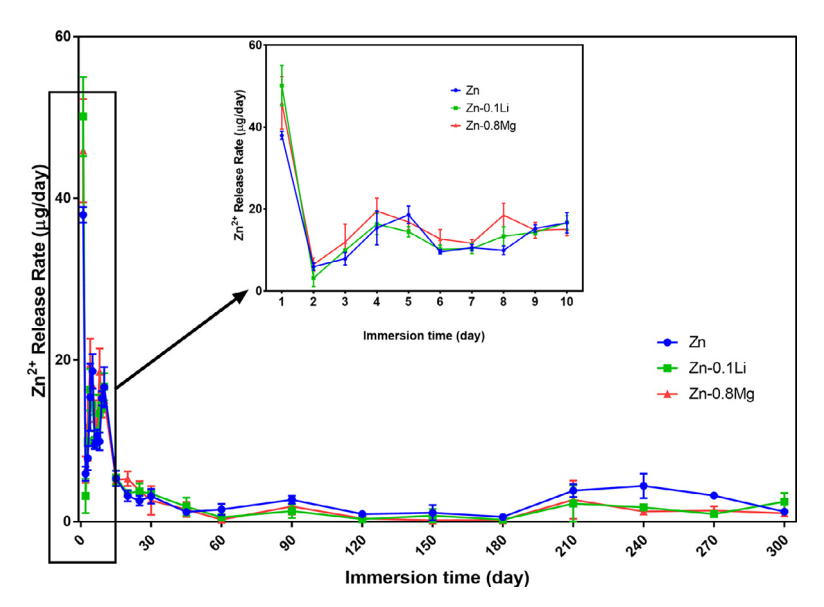
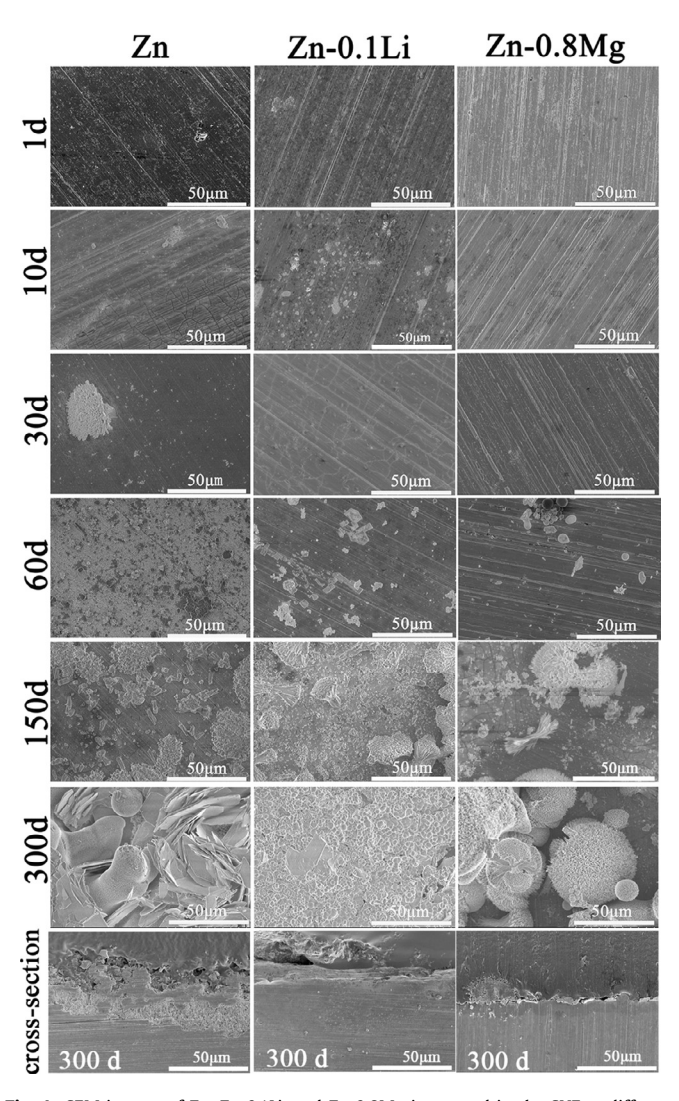


Fig. 3. Zinc ion concentrations of Zn, Zn-0.1Li, and Zn-0.8Mg at different immersion time points. The line chart represents mean \pm SD; n=3.

Table 2 The parameters of open circuit potential, E_{corr} , i_{corr} , and corrosion rates for Zn, Zn-0.1Li, and Zn-0.8Mg in the SUF.

	Open circuit potential (V_{SCE})	E _{corr} (V vs.SCE)	$i_{corr}\ (\mu A/cm^2)$	Corrosion rate (mm/y)
Zn Zn-0.1Li Zn-0.8Mg	$\begin{array}{l} -1.051 \pm 0.031 \\ -1.027 \pm 0.006 \\ -1.028 \pm 0.001 \end{array}$	$\begin{array}{l} -1.236 \pm 0.021 \\ -1.052 \pm 0.026^* \\ -1.047 \pm 0.022^* \end{array}$	$\begin{array}{c} 2.272\pm0.347 \\ 0.142\pm0.031^* \\ 0.154\pm0.081^* \end{array}$	$\begin{array}{c} 0.141 \pm 0.021 \\ 0.088 \pm 0.002^* \\ 0.095 \pm 0.005^* \end{array}$

The symbol * represents statistically significantly different from the Zn group.



 $\begin{tabular}{ll} \textbf{Fig. 4.} SEM images of Zn, Zn-0.1Li, and Zn-0.8Mg immersed in the SUF at different time points. \end{tabular}$

no significant difference was observed between the Zn-0.1Li and Zn-0.8Mg groups.

3.4. In vitro cytocompatibility studies

Fig. 7a-c present the cell viabilities in the extracted media for the Zn, Zn-0.1Li, and Zn-0.8Mg groups. The three material extracts exhibited different effects on the cell viability of the tested cell types. The HEECs (Fig. 7b) showed significantly lower cell viabilities in the presence of Zn extracts than those in the presence of Zn-0.1Li and Zn-0.8Mg. The HUSMCs (Fig. 7a) presented cell viabilities with no significant differences among the three groups. In addition, the cell viabilities were increased on Day 5 compared to those on Day 1 and Day 3. The HESCs (Fig. 7c) presented slightly

higher cell viabilities in the presence of Zn-0.1Li and Zn-0.8Mg extracts compared to those in the presence of Zn. The variations in the pH of the cell culture media in the presence of the three material extracts were monitored, and the results are presented in Fig. 7d. The extracts from the Zn, Zn-0.1Li, and Zn-0.8Mg groups induced the alkalinization of the complete DMEM medium, as evidenced by the significant increase in the pH values from 7.45 to 7.76 for the Zn group (P < 0.01), to 7.82 for the Zn-0.1Li group (P < 0.01), and to 7.84 for the Zn-0.8Mg group (P < 0.01). Under the complete DMEM condition, the pH values did not differ significantly between the Zn-0.1Li and Zn-0.8Mg groups. Moreover, the pH value of the Zn-0.8Mg group was clearly distinguishable from and significantly higher than that of the Zn group (P < 0.05). Furthermore, under the DMEM/F12 medium condition, the pH values remained almost unchanged prior to and after the preparation of the experimental material extracts. The metal ion concentrations of the cell culture media in the presence of the Zn, Zn-0.1Li, and Zn-0.8Mg group extracts are listed in Table 3. The concentration of Zn²⁺ in the Zn group was higher than that in the Zn-0.1Li and Zn-0.8Mg groups under all three cell culture media conditions.

3.5. In vivo animal experiment

To investigate the effects of tissue response to the implantation, rod samples from the Zn, Zn-0.1Li, and Zn-0.8Mg groups were implanted into the rat uterine cavity. The schematic diagram for the implantation of materials and collection sites is presented in Fig. S3. The time points of 3, 7, 14, and 28 days after implantation were selected for obtaining tissue samples for examination. No obvious distinction could be observed in the uterine surface between the normal and the implanted-material groups. Fig. 8 illustrates the inflammatory response at different implantation sites and at different implantation time points for the Zn, Zn-0.1Li, and Zn-0.8Mg groups. A significant acute inflammatory reaction was detected on Day 3 in the endometrial area where the materials were touching directly [the arrows indicate a significant increase in neutrophils in the area]. The lower part of the right uterine tissue where the materials did not touch remained normal as the left uterine tissue. The inflammatory cells were mainly eosinophils. On Day 7, after the implantation, the inflammatory reactions could still be observed in the form of neutrophil leaching, and the number of inflammatory cells in the endometrium of the lower part without the direct touching section was significantly higher than that on Day 3. These results implied that the accumulation of Zn ions and corrosion products may activate the immune system. A significant reduction in the inflammatory reaction involving neutrophils was observed on Day 14, although with a significant simultaneous increase in the lymphocytes, indicating that the endometrium underwent a chronic inflammatory reaction. Squamous epithelialization also occurred in some of the endometrial glands. On Day 28, the endometrial tissue exhibited lymphocytic infiltration, indicating a chronic inflammatory response within the endometrium. The counting of inflammatory cells showed that the pure zinc group had significantly higher count of inflammatory cells than the other two alloys, as shown in Fig. 8d. Overall, it was demonstrated that

Table 3 Ion concentrations of Zn, Zn-0.1Li, and Zn-0.8Mg immersed in the culture medium (DMEM or DMEM/F12 + 10% FBS + 100 U·mL⁻¹ penicillin and 100 g·mL⁻¹ streptomycin) for 24 h. (mean \pm SD; n=3). **P<0.01. Zn-0.1Li and Zn-0.8Mg groups compared with the Zn group.

Extracts	Zn (μM) Zn	Zn-0.1Li	Zn-0.8Mg	Li (μM) Zn-0.1Li	Mg (μM) Zn-0.8Mg
HUSMC HEEC/HESC Normal culture media HUSMC HEEC/HESC	$\begin{array}{c} 188.88 \pm 8.86 \\ 182.30 \pm 16.02 \\ \text{Zn } (\mu\text{M}) \\ 3.96 \pm 0.51 \\ 8.99 \pm 0.53 \end{array}$	135.23 ± 13.43** 155.28 ± 18.06	$\begin{array}{c} 129.37\pm10.67^{**} \\ 154.08\pm10.69 \\ \text{Li } (\mu\text{M}) \\ 0.40\pm0.27 \\ 0.20\pm0.04 \end{array}$	143.38 ± 3.72 117.10 ± 12.31	$766.20 \pm 17.29 \\ 697.50 \pm 15.11 \\ Mg (\mu M) \\ 757.44 \pm 18.53 \\ 708.07 \pm 23.20$

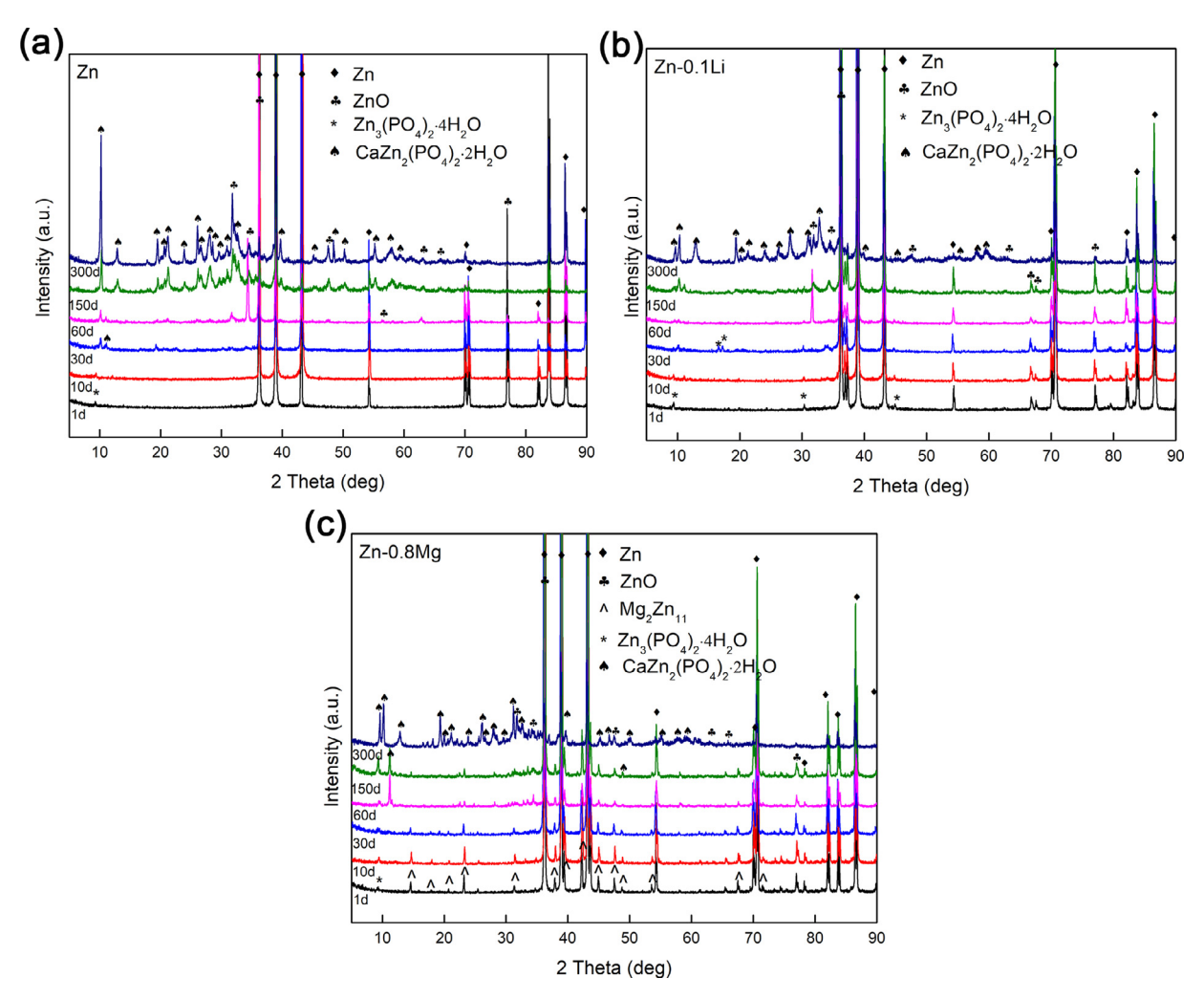


Fig. 5. XRD patterns of (a) Zn, (b) Zn-0.1Li, and (c) Zn-0.8Mg immersed in the SUF at different time points.

the effects on the endometrial inflammatory response observed for the Zn group were more severe than those observed for the two Zn alloy groups. To more clearly observe the inflammatory response, we examined the inflammatory cells in the tissue with CD45 antibodies, as shown in Fig. S4. The image shows inflammatory cells with arrows, and the inflammatory response of the zinc alloys was lighter.

Furthermore, the surface corrosion morphologies of the three kinds of experimental materials were observed at the same time points (Fig. 9). The SEM results revealed a gradual increase in the corrosion product layers on the surface of the implanted Zn, Zn-0.1Li, and Zn-0.8Mg rods with increasing implantation time dura-

tion within the rat's uterine cavity. The Zn group surface showed the formation of flaky corrosion products, while the Zn-0.8Mg group showed loose spongy mesh corrosion products. The flaky corrosion products on the rod surface in the Zn group became further condensed on Day 28. The corrosion products formed after implantation were also analyzed through XRD (Fig. 10). The major peaks detected could be attributed to the zinc matrix phase. Moreover, weak peaks corresponding to the ZnO phase were observed at different implantation times for all three experimental materials. Different from the *in vitro* immersion experiments, in the *in vivo* experiments, the diffraction peaks of the CaCO₃ phase were detected on the surface of the Zn, Zn-0.1Li, and Zn-0.8Mg rods im-

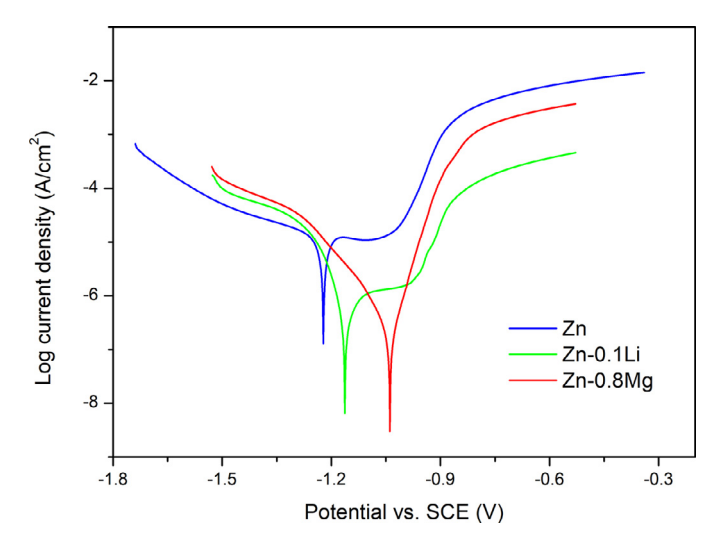


Fig. 6. Potentiodynamic polarization curves for Zn, Zn-0.1Li, and Zn-0.8Mg in the SUF.

planted in the SD rat's uterine cavity, possibly due to the presence of proteins, cells, and other organic substances around the implanted rods, demonstrating that the *in vivo* chemical reaction

occurring in the vicinity of the implanted materials differed from the reaction that occurred during the *in vitro* immersion tests.

4. Discussion

4.1. Degradation behaviors of Zn and its alloys in the uterine microenvironment

In the present study, SUF was used as the corrosion medium to simulate the uterine microenvironment and to evaluate its effects on zinc and its alloys. Generally, the initial oxidation of zinc occurs via the anodic and cathodic reactions represented by Eq(1) and Eq(2), respectively [31]. The results of the present study revealed a significant increase in the pH and Zn^{2+} concentrations of the SUF during the initial stages of immersion (Figs. 1 and 3, respectively). Simultaneous formation of ZnO and Zn(OH)2 occurs upon the increase in the pH and Zn^{2+} concentrations [12,32-34], as represented by Eq. (3) and Eq. (4). The monitoring of the pH variation in the SUF for the 300 days of immersion revealed that the pH did not reach beyond 11, favoring the formation of ZnO [35,36], which was consistent with the XRD patterns (Fig. 5) that indicated the absence of Zn(OH)₂ in the corrosion products. A comparison of the compositions of the SUF and other SBFs is provided in Table 4 [24]. There are three types of anions in the SUF: chlorine, bicarbonate, and dihydrogen phosphate. The chlorine ions from the

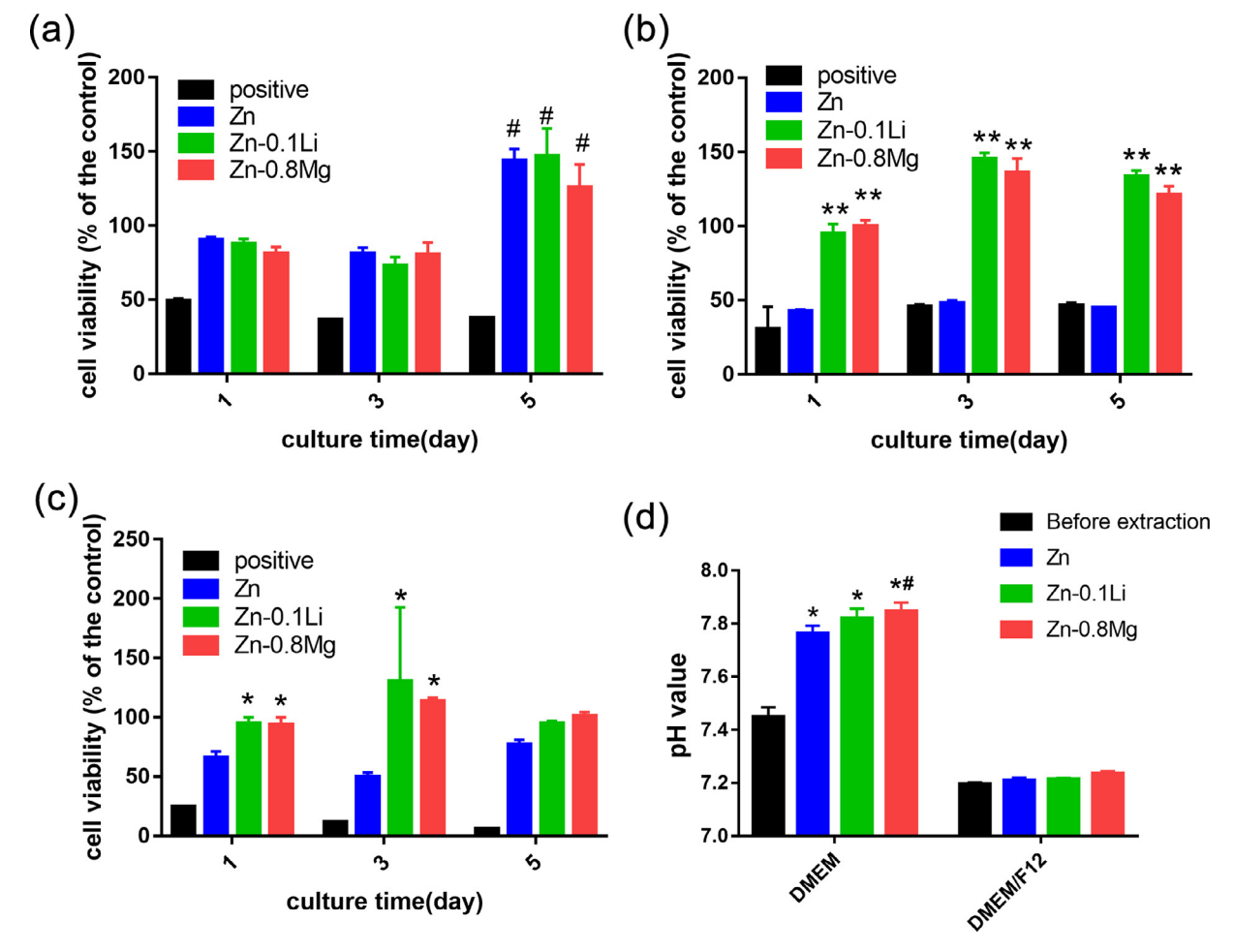


Fig. 7. Viabilities of (a) HUSMCs, (b) HEECs, and (c) HESCs after 1, 3, and 5 days of incubation, for Zn, Zn-0.1Li, and Zn-0.8Mg group extracts, normal medium, and normal (negative control) with 10% DMSO (positive control). The bar graph represents mean \pm SD; n = 5, *P < 0.05; **P < 0.01, each time point and each group compared with the positive control; # P < 0.05, Day 5 of each group compared with Day 1 and Day 3 in (a). (d) pH of DMEM and DMEM/F12 extracts prior to and after the experiment. The bar graph represents mean \pm SD; n = 5, *P < 0.05 each extraction group compared with the results prior to the extraction, # P < 0.05 Zn-0.8Mg group compared with the Zn group. (For interpretation of the references to colour in this figure legend, the reader is referred to the web version of this article.)

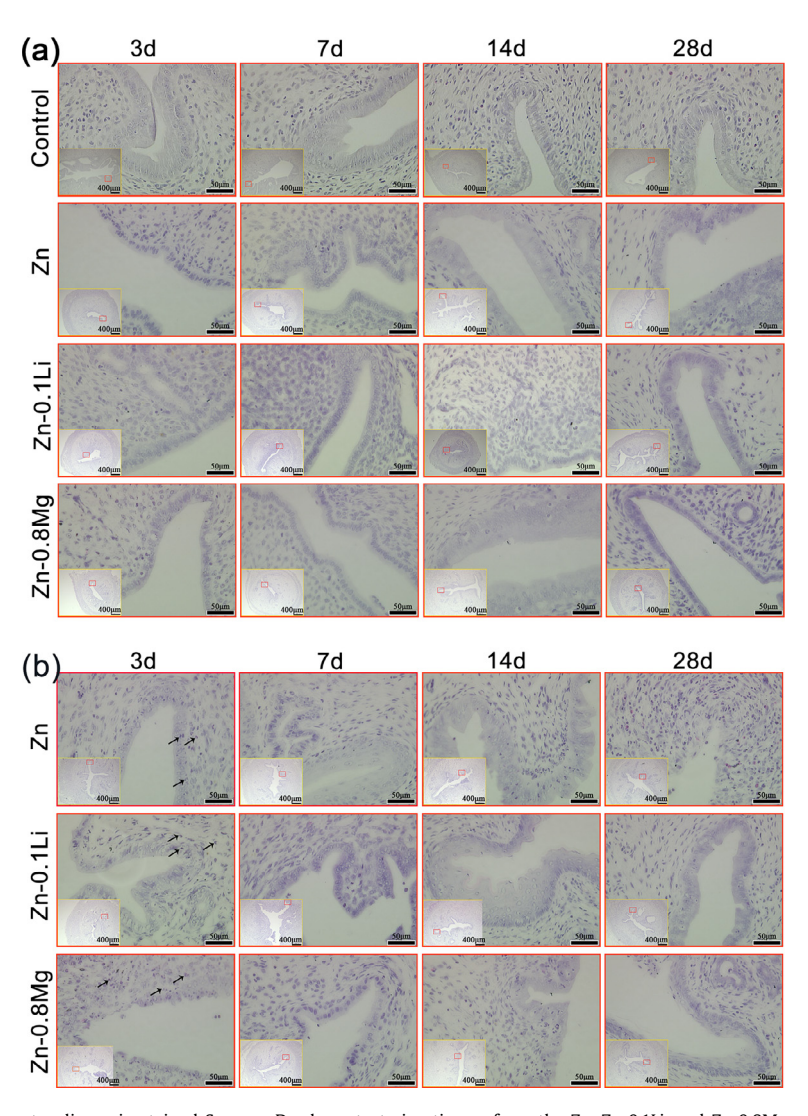


Fig. 8. Histological images of the hematoxylin-eosin-stained Sprague-Dawley rat uterine tissues from the Zn, Zn-0.1Li, and Zn-0.8Mg groups after implantation for 3, 7, 14, and 28 days. (a) Materials implanted in the contralateral uterine tissue and the non-implanted materials (control), (b) direct contact with the uterine tissue, and (c) the lower uterine tissue with the implant (no contact with the material). (d) The number of inflammatory cells of the pure Zn, Zn-0.1Li, and Zn-0.8Mg alloy groups. The bar graph represents mean \pm SD; n = 5, *P < 0.05.

SUF attack the hydroxide, as represented by Eq (5). In the initial stage of immersion, Zn₃(PO₄)₂·4H₂O was detected in the corrosion products through XRD; the formation of Zn₃(PO₄)₂·4H₂O is represented by Eq (6). A previous study reported the presence of $Zn_3(PO_4)_2 \cdot 4H_2O$ when zinc was exposed to PBS [31]. Other studies reported $Zn_5(CO_3)_2(OH)_6$ or $Zn_4(CO_3)(OH)_6 \cdot H_2O$ as the corrosion products of zinc under the SUF immersion conditions. Chen et al. demonstrated that the nature of corrosion products relied strongly on the CO_2 concentration [37]. In the present study, the experimental samples were immersed inside sealed centrifuge tubes, which might have led to the absence of zinc hydroxide carbonate among the corrosion products. The EDS results of the present study revealed Zn, O, P, and Ca as the main elements in the corrosion products, while the other elements such as C and Mg were not detected [38]. Gong et al.[39]. reported that the top layer of the biodegradation products of Zn-1Mg alloy immersed in the SBF was mainly composed of Zn, O, P, and Ca. Another study focused on the application of Zn-Mg alloys in artificial urine also revealed that the corrosion products did not contain Mg [40]. Moreover, in the present study, CaZn₂(PO₄)₂·2H₂O appeared in the corrosion product layer after long-term immersion in the SUF.

$$Zn(s) \to Zn^{2+}(aq) + 2e^{-} \tag{1}$$

$$2H_2O + O_2 + 4e^- \rightarrow 4OH^-$$
 (2)

$$Zn^{2+} + 2OH^{-} \rightarrow Zn(OH)_{2}$$
 (3)

$$Zn^{2+} + 20H^{-} \rightarrow ZnO + H_2O$$
 (4)

$$Zn(OH)_2 + 2Cl^- \rightarrow Zn^{2+} + 2OH^- - +2Cl^-$$
 (5)

$$3Zn^{2+} + 2H_2PO^- + 4OH^- \rightarrow Zn_3(PO_4)_2 \cdot 4H_2O$$
 (6)

In comparison to the *in vitro* immersion experiment results, the *in vivo* experiment results revealed CaCO₃ and ZnO to be the main constituents of the surface corrosion layer of zinc and its alloys implanted in the rat uterine cavities. Previous studies have also reported CaCO₃ to be a common constituent of the corrosion layer attached to the surface of the material in certain intrauterine implants such as IUDs [41]. In other studies, such as our previous study [24] and certain studies on zinc in Hank's solution [12,15],

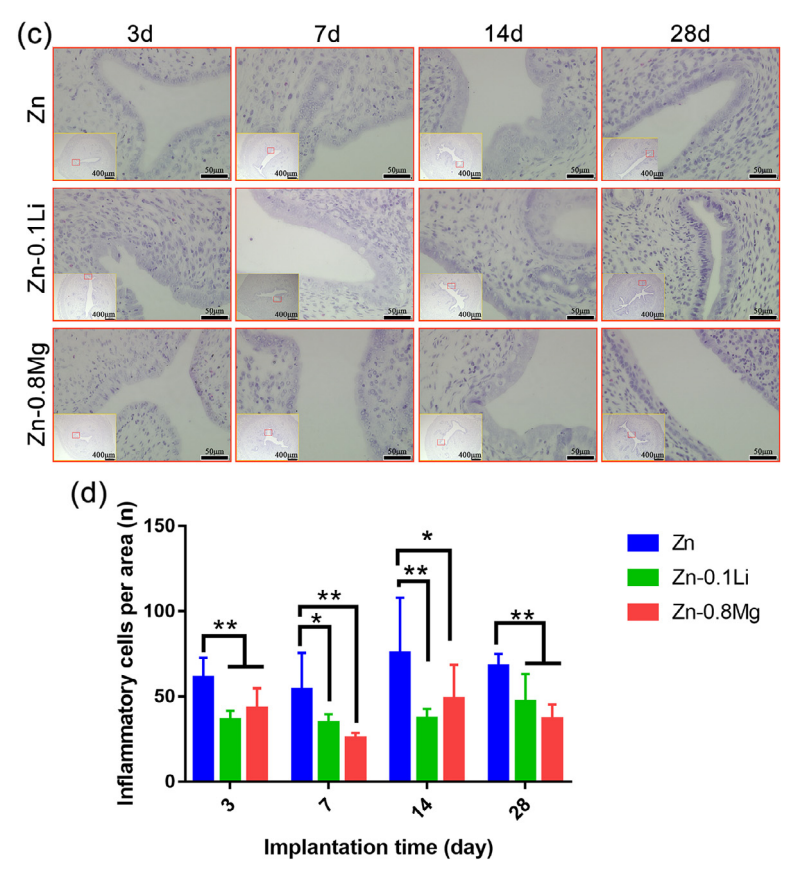
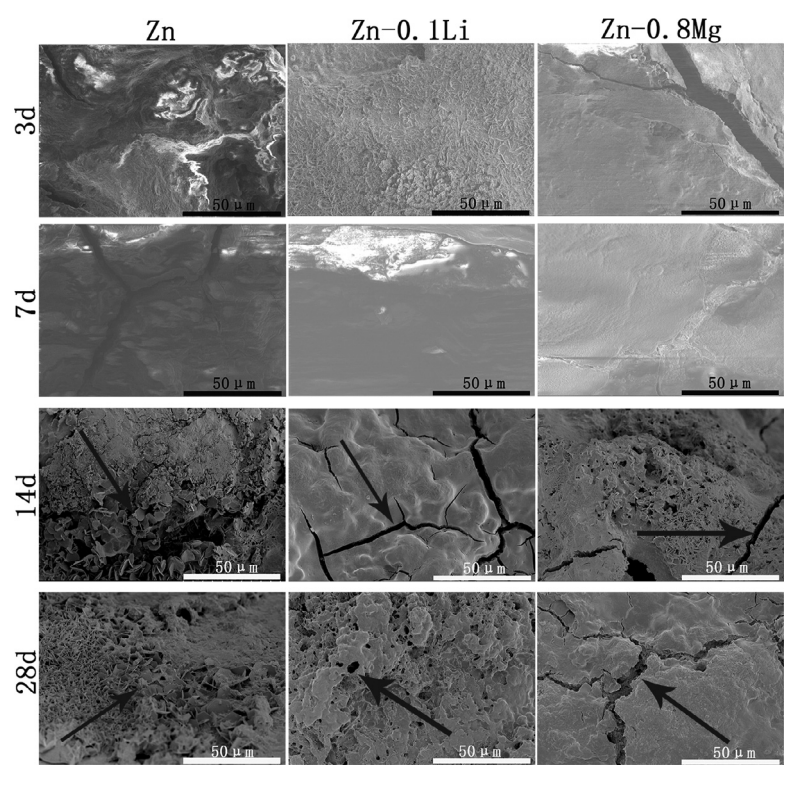


Fig. 8. Continued



 $\textbf{Fig. 9.} \ \ \textbf{SEM} \ \ images \ for \ the \ Zn-0.1Li, \ and \ Zn-0.8Mg \ groups \ \ after \ implantation \ for \ 3, \ 7, \ 14, \ and \ 28 \ days.$

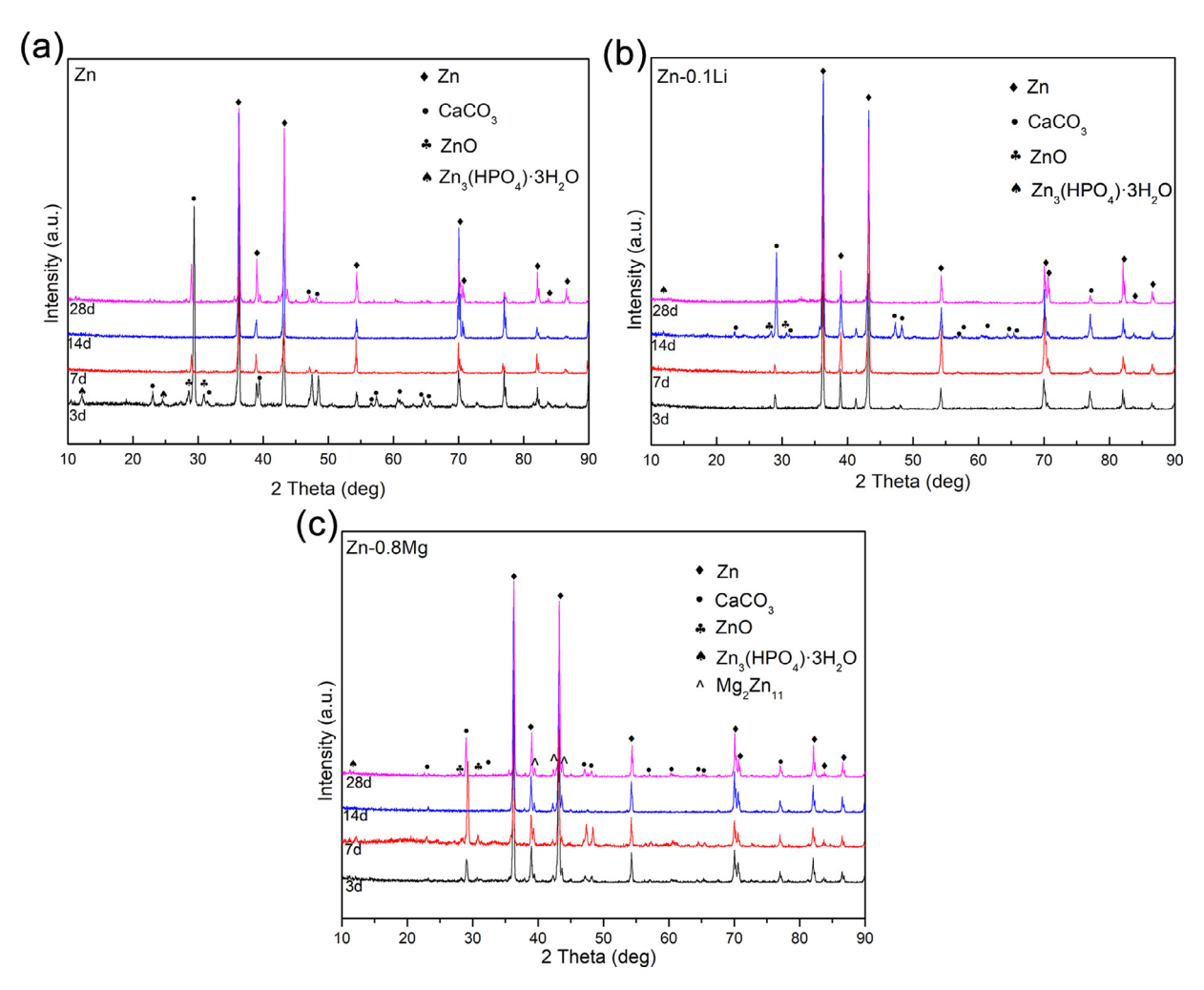


Fig. 10. XRD patterns for the (a) Zn, (b) Zn-0.1Li, and (c) Zn-0.8Mg groups after implantation for 3, 7, 14, and 28 days.

 ${\rm CaCO_3}$ appeared in the corrosion product layer in certain *in vitro* immersion experiments. The presence of ${\rm Zn}({\rm HPO_4}) \cdot {\rm 3H_2O}$ has also been detected in the corrosion product layers of the experimental samples implanted in animals. It is well recognized that due to the microcirculation in the body, the internal environment of the body maintains a relatively stable state as compared to the *in vitro* environment and might be responsible for the formation of different products in the same chemical reaction occurring *in vivo* and *in vitro*.

It is clear from the surface morphologies of the materials (Fig. 4) that the Zn surface had more corrosion products. The Zn surface presented only a few visible corrosion spots after immersion for 10 days, which increased with the increasing immersion duration. Conversely, the Zn-0.8Mg and Zn-0.1Li alloy surfaces presented large areas covered uniformly with the corrosion products. The XRD results revealed a second phase-Mg₂Zn₁₁-in the Zn-0.8Mg alloy, which could lead to variation in the grain sizes [42]. The finer regular structure of Zn-0.8Mg compared to that of Zn could lead to more uniformly spread corrosion, thereby enhancing resistance [43]. Although the intermetallic LiZn₄ phase was not detected in the present study, certain previous studies have reported the presence of LiZn₄ in Zn-Li alloys, which may improve the corrosion behavior of zinc [28,44]. As depicted in Fig. 5, after long-term immersion, the corrosion products formed a phosphate corrosion layer, and the new phosphate corrosion layer was formed after the release of new phosphate ions caused by the change of solution. The corrosion rates were determined 28 days

after the implantation, and the pure Zn, Zn-0.1Li, and Zn-0.8Mg implants showed the corrosion rates of 0.047 mm/y, 0.045 mm/y, and 0.039 mm/y, respectively. The corrosion rates after the *in vivo* implantation into the uterine cavity were higher than those observed in the *in vitro* immersion tests. Previously, when Zn was used as the implanted material, its corrosion rate was accelerated due to the presence of certain minor constituents of the uterine fluid, such as sulfur contained in amino acids [45]. The inflammatory reactions were also reported to increase the corrosion rate of Zn alloys [46]. Therefore, it is possible that in the present study, the uterine environment and the chronic inflammation occurring around the implanted Zn materials accelerated the degradation process of the Zn alloys.

4.2. Biocompatibility of Zn and its alloys in the uterine microenvironment

To determine the potential and feasibility of the candidate material for biomedical application in the uterine microenvironment, biocompatibility is an important evaluation factor. The interaction of the implant material with the surrounding uterine tissue must be considered. The uterine tissue comprises multiple cell types, including HEECs, HESCs, and HUSMCs. In the present study, the effects of the extracts of three experimental [Zn and its alloys] materials on the viability of uterine cells were investigated. Previous studies conducted on Zn and its alloys focused on the use of stents and orthopedic implants, and thus, the *in vitro* cytotox-

on concentrations in the simulated uterine fluid (SUF) and the other simulated environments or cell culture media

			()									
Media	Na+(mmol/L)	K+(mmol/L)	Ca+(mmol/L)	$Na^+(mmol/L) K^+(mmol/L) Ca^+(mmol/L) Mg^{2+}(mmol/L)$	Cl-(mmol/L)	HCO ₃ (mmol/L)	$H_2PO_4^-(mmol/L)$	$HPO_4^{2-}(mmol/L)$	$SO_4^{2-}(mmol/L)$	Glucose(g/L)	$ \text{CI-}(\text{mmol/L}) \text{HCO}_3^-(\text{mmol/L}) \text{H2PO}_4^-(\text{mmol/L}) \text{SO}_4^2^-(\text{mmol/L}) \text{Glucose}(g/L) \text{Amino acids}(\text{mg/L}) \text{pH} $	Hd
SUF	88.5	3.0	1.5	1	91.0	3.0	0.5	1	1	1.0		6.0-7.9
Plasma	142.0	5.0	2.5	1.5	103.0	27.0		1.0	0.5			7.35-7.45
SBF	142.0	5.0	2.5	1.5	148.5	4.2		1.0	0.5			7.35-7.45
m-SBF	142.0	5.0	2.5	1.5	103.0	10.0		1.0	0.5			7.35-7.45
Hank's	145.0	5.8	1.3	0.4	144.6	26.2		8.0	0.4	5.5		7.2-7.4
Earle(+)	151.0	5.4	1.8	8.0	125.0	26.2	6.0		8.0	1.0	6.0	7.2-7.4
E-MEM	151.0	5.4	1.8	8.0	125.0	26.2	6.0	1	0.8	1.1	6.0	7.2-7.4
DMEM	154.9	5.3	1.8	8.0	118.9	44.0	6.0	ı	0.8	25	6.0	7.2-7.4

icity evaluations were usually conducted in bone cells and blood vessel cells. A study reported that LD_{50} at the Zn^{2+} concentration of 300 µM in the primary human aortic endothelial cells (EC) and at the Zn²⁺ concentration of 280 µM in the primary human aortic smooth muscle cells (SC) [47]. Shearer et al. performed aqueous cytotoxicity studies using a Zn²⁺ salt assay and reported LD₅₀ values of 50 µM for human dermal fibroblasts (hDF), 70 µM for human aortic smooth muscle cells (AoSMC), and 265 µM for human aortic endothelial cells (HAEC) [19]. In the present study, the experimental Zn and its alloys could induce diverse responses in the three types of uterine cells. In the HUSMCs, although the pH values of the extracts increased significantly (Fig. 7a), no inhibition of the cell viabilities was observed. A wide pH range of 6.0 to 7.9 was observed for the uterine fluid, with the pH varying in parallel with the menstrual physiological cycle [48]. The pH of the extracts did not exceed 7.9 in DMEM. However, in HEECs and HESCs, the Zn extracts inhibited the cell viabilities, while the Zn-0.8Mg and Zn-0.1Li extracts effectively improved cytocompatibility. Lower Zn²⁺ concentrations might be one of the reasons for the lower cytotoxicity of the Zn-0.1Li and Zn-0.8Mg extracts, as there was no significant difference in the pH values of these extracts (Fig. 7d).

When the experimental zinc materials were implanted into the uterine cavity in the present study, an acute inflammatory reaction occurred, particularly in the first three days, which was induced due to direct contact with the implanted material. The lower part of the uterine corner exhibited a mild reaction, while no differences were observed between the uterine tissue on the side and the uterine tissue not in contact with the experimental zinc materials. Therefore, it is evident that either the ion concentration or the corrosion products formed on the surface at the site of material contact induce the inflammatory response in the uterine tissue. The mechanical friction occurring due to contact with the implanted material could also be one of the factors causing the change in the morphology of the uterine tissue. After longer implantation durations, a chronic inflammatory response appeared to occur in the uterine tissue, indicating the infiltration of inflammatory cells, mainly lymphocytes. In addition, a scaly growth in the endometrial adrenal epithelial cells was observed. Overall, the inflammatory responses observed in the Zn-0.1Li and Zn-0.8Mg groups were slightly weaker than that observed in the Zn group, reflecting the better biocompatibility of the former materials. Moreover, the results of the *in vivo* implantation experiment were consistent with the findings of the in vitro cytotoxicity assays evaluating the response of various uterine cells. Although Zn-0.1Li and Zn-0.8Mg caused mild chronic inflammation when implanted into the uterine side, they exhibited better biocompatibilities than pure Zn. It is recommended that future research should include methods such as surface modification to control the release of zinc ions and the degradation rate, which would improve the biocompatibility of the experimental alloys and render them further efficient as potential candidates for biomedical and implantation applications.

5. Conclusions

In the present study, the biodegradation behaviors of Zn, Zn-0.1Li, and Zn-0.8Mg in the SUF were investigated. In addition, the biocompatibilities of these materials were evaluated through *in vitro* and *in vivo* [implantation in the rat uterine cavity] cytotoxicity experiments. The Zn alloys could effectively decrease the degradation rate of zinc and improved the biocompatibilities both *in vitro* and *in vivo*. The cell cytotoxicity assays provided evidence of a good cytocompatibility of the Zn-0.1Li and Zn-0.8Mg alloys. The *in vivo* experiments demonstrated that both Zn-0.1Li and Zn-0.8Mg alloys caused less inflammation in the uterine tissue than pure Zn.

According to the experimental results, the following conclusions were drawn.

- (1) ZnO was formed as the main corrosion product during the degradation of Zn, Zn-0.1Li, and Zn-0.8Mg in the uterine environment. In addition, Zn₃(PO₄)₂·4H₂O and CaZn₂(PO₄)₂·2H₂O were formed *in vitro*, while CaCO₃ and Zn(HPO₄)·3H₂O were formed *in vivo*.
- (2) In comparison to Zn, the Zn-0.1Li and Zn-0.8Mg alloys induced less cytotoxicity in the uterine cells (HUSMCs, HEECs, and HESCs) *in vitro*.
- (3) In comparison to Zn, both Zn-0.1Li and Zn-0.8Mg caused weaker inflammatory reactions in the uterine tissue after implantation, and their recovery period was also short.
- (4) The Zn alloys exhibited better biocompatibilities than pure Zn, and are therefore recommended as promising candidate materials for intrauterine medical device applications.

Declaration of Competing Interest

The authors declare that they have no known competing financial interests or personal relationships that could have appeared to influence the work reported in this paper.

Acknowledgments

This work was supported by the National Key R&D Program of China (grant no. 2016YFC1000903), CAMS Innovation Fund for Medical Sciences (CIFMS) (grant no. 2018-I2M-1-004), the Nonprofit Central Research Institute Fund of National Research Institute For Family Planning (grant no. 2020GJZ07), and National Natural Science Foundation of China (grant no. 51931001).

Supplementary materials

Supplementary material associated with this article can be found, in the online version, at doi:10.1016/j.actbio.2020.12.048.

References

- [1] W. Maret, Analyzing free zinc(II) ion concentrations in cell biology with fluorescent chelating molecules, Metallomics 7 (2015) 202–211.
- [2] J.E. Coleman, Zinc proteins: enzymes, storage proteins, transcription factors, and replication proteins, Annu. Rev. Biochem. 61 (1992) 897–946.
- [3] L. Rink, P. Gabriel, Zinc and the immune system, Proc. Nutr. Soc. 59 (2000)
- [4] B.B. Mcallister, R.H. Dyck, Zinc Transporter 3 (ZnT3) and vesicular zinc in central nervous system function, Neuro. Biobehav. Rev. 80 (2017) 329–350.
- [5] I.M.W. Ebisch, C.M.G. Thomas, W.H.M. Peters, D.D.M. Braat, R.P.M. Steegers-Theunissen, The importance of folate, zinc and antioxidants in the pathogenesis and prevention of subfertility, Hum. Reprod. Update. 13 (2007) 163–174.
- [6] P.H. Lin, M. Sermersheim, H. Li, P.H.U. Lee, S.M. Steinberg, J. Ma, Zinc in wound healing modulation, Nutrients 10 (2017) 1–20.
- [7] A.S. Prasad, Clinical, immunological, anti-inflammatory and antioxidant roles of zinc, Exp. Gerontol. 43 (2008) 370–377.
- [8] H.R. Bakhsheshi-Rad, E. Hamzah, H.T. Low, M. Kasiri-Asgarani, S. Farahany, E. Akbari, M.H. Cho, Fabrication of biodegradable Zn-Al-Mg alloy: mechanical properties, corrosion behavior, cytotoxicity and antibacterial activities, Mater. Sci. Eng. C-Mater. Biol. Appl. 73 (2017) 215–219.
- [9] P.K. Bowen, J. Drelich, J. Goldman, Zinc exhibits ideal physiological corrosion behavior for bioabsorbable stents, Adv. Mater. 25 (2013) 2577–2582.
- [10] P.K. Bowen, R.J. Guillory, E.R. Shearier, J.M. Seitz, J. Drelich, M. Bocks, F. Zhao, J. Goldman, Metallic zinc exhibits optimal biocompatibility for bioabsorbable endovascular stents, Mater. Sci. Eng. C-Mater. Biol. Appl. 56 (2015) 467–472.
- [11] K.B. Törne, A. Örnberg, J. Weissenrieder, Characterization of the protective layer formed on zinc in whole blood. Electrochim. Acta. 258 (2017) 1476–1483.
- [12] H. Guo, D.D. Xia, Y.F. Zheng, Y. Zhu, Y.S. Liu, Y.S. Zhou, A pure zinc membrane with degradability and osteogenesis promotion for guided bone regeneration: *in vitro* and *in vivo* studies, Acta Biomater. 106 (2020) 396–409.
- [13] K. Torne, M. Larsson, A. Norlin, J. Weissenrieder, Degradation of zinc in saline solutions, plasma, and whole blood, J. Biomed. Mater. Res. Part B. 104 (2016) 1141–1151.
- [14] W. Yuan, D.D. Xia, Y.F. Zheng, X.W. Liu, S.L. Wu, B. Li, Y. Han, Z.J. Jia, D.H. Zhu, L.Q. Ruan, K. Takashima, Y.S. Liu, Y.S. Zhou, Controllable biodegradation and enhanced osseointegration of ZrO₂-nanofilm coated Zn-Li alloy: *in vitro* and *in vivo* studies, Acta Biomater 105 (2020) 290–303.

[15] H.T. Yang, X.H. Qu, W.J. Lin, C. Wang, D.H. Zhu, K.R. Dai, Y.F. Zheng, In vitro and in vivo studies on zinc-hydroxyapatite composites as novel biodegradable metal matrix composite for orthopedic applications, Acta Biomater. 71 (2018) 200–214.

- [16] D.H. Zhu, Y.C. Su, M.L. Young, J. Ma, Y.F. Zheng, L.P. Tang, Biological responses and mechanisms of human bone marrow mesenchymal stem cells to Zn and Mg biomaterials, ACS Appl. Mater. Interfaces. 33 (2017) 27453–27461.
- [17] J. Ma, N. Zhao, D.H. Zhu, Endothelial cellular responses to biodegradable metal zinc, ACS Biomater. Sci. Eng. 1 (2015) 1174–1182.
- [18] J. Ma, N. Zhao, D.H. Zhu, Biphasic responses of human vascular smooth muscle cells to magnesium ion released from magnesium biomaterials, J. Biomed. Mater. Res. Part A. 104 (2015) 347–356.
- [19] E.R. Shearier, P.K. Bowen, W.L. He, A. Drelich, J. Drelich, J. Goldman, F. Zhao, In vitro cytotoxicity, adhesion, and proliferation of human vascular cells exposed to zinc, ACS Biomater. Sci. Eng. 2 (2016) 634–642.
- [20] K.N. Khan, A. Fujishita, M. Kitajima, K. Hiraki, M. Nakashima, H. Masuzaki, Intra-uterine microbial colonization and occurrence of endometritis in women with endometriosis, Hum. Reprod. 29 (2014) 2446–2456.
- [21] J.Y. Liang, Y. Li, X. Gu, Y.L. Gao, H.P. Liu, Investigation of the release behavior of cupric ion for three types of Cu-IUDs and indomethacin for medicated Cu-IUD in simulated uterine fluid, Contraception 77 (2008) 299–302.
- [22] E.N. Berry-Bibee, N.K. Tepper, T.C. Jatlaoui, M.K. Whiteman, D.J. Jamieson, K.M. Curtis, The safety of intrauterine devices in breastfeeding women: a systematic review, Contraception 94 (2016) 725–738.
- [23] C.S. Chiu, Y.M. Hwu, R.K. Lee, M.H. Lin, Intrauterine adhesion prevention with Malecot catheter after hysteroscopic myomectomy: a novel approach, Taiwan. J. Obstet. Gynecol. 59 (2020) 56–60.
- [24] G. Bao, Q.Q. Fan, D.F. Ge, M.M. Sun, H. Guo, D.D. Xia, Y. Liu, J.N. Liu, S.C. Wu, B. He, Y.F. Zheng, *In vitro* and *in vivo* studies on magnesium alloys to evaluate the feasibility of their use in obstetrics and gynecology, Acta Biomater. 97 (2019) 623–636.
- [25] J. Kubasek, D. Vojtech, E. Jablonska, I. Pospisilova, J. Lipov, T. Ruml, Structure, mechanical characteristics and in vitro degradation, cytotoxicity, genotoxicity and mutagenicity of novel biodegradable Zn-Mg alloys, Mater. Sci. Eng. C– Mater. Biol. Appl. 58 (2016) 24–35.
- [26] H.F. Li, X.H. Xie, Y.F. Zheng, Y. Cong, F.Y. Zhou, K.J. Qiu, X. Wang, S.H. Chen, L. Huang, L. Tian, L. Qin, Development of biodegradable Zn-1X binary alloys with nutrient alloying elements Mg, Ca and Sr, Sci. Rep. 5 (2015) 1–13.
- [27] W. Young, Review of lithium effects on brain and blood, Cell Transplant. 18 (2009) 951–975.
- [28] S. Zhao, J.M. Seitz, R. Eifler, H.J. Maier, R.J. Guillory, E.J. Earley, A. Drelich, J. Goldman, J.W. Drelich, Zn-Li alloy after extrusion and drawing: structural, mechanical characterization, and biodegradation in abdominal aorta of rat, Mater. Sci. Eng. C-Mater. Biol. Appl. 76 (2017) 301–312.
- [29] H.T. Yang, B. Jia, Z.C. Zhang, X.H. Qu, G.N. Li, W.J. Lin, D.H. Zhu, K.R. Dai, Y.F. Zheng, Alloying design of biodegradable zinc as promising bone implants for load-bearing applications, Nat. Commun. 11 (2020) 1–16.
- [30] ASTM G31 -72, Standard Practice For Laboratory Immersion Corrosion Testing of Metals, ASTM International, Philadelphia West Conshohocken, PA, 2004.
- [31] P. Li, J.T. Dai, E. Schweizer, F. Rupp, A. Heiss, A. Richter, U.E. Klotz, J. Geis-Gerstorfer, L. Scheideler, D. Alexander, Response of human periosteal cells to degradation products of zinc and its alloy, Mater. Sci. Eng. C-Mater. Biol. Appl. 108 (2020) 110208 doi.org/10.1016/j.msec.2019.110208.
- [32] Y.Q. Chen, W.T. Zhang, M.F. Maitz, M.Y. Chen, H. Zhang, J.L. Mao, Y.C. Zhao, N. Huang, G.J. Wan, Comparative corrosion behavior of Zn with Fe and Mg in the course of immersion degradation in phosphate buffered saline, Corros. Sci. 111 (2016) 541–555.
- [33] M.A. Amin, Passivity and passivity breakdown of a zinc electrode in aerated neutral sodium nitrate solutions, Electrochim. Acta 50 (2005) 1265–1274.
- [34] L.C. Zhao, Z. Zhang, Y.T. Song, S.J. Liu, Y.M. Qi, X. Wang, Q.Z. Wang, C.X. Cui, Mechanical properties and in vitro biodegradation of newly developed porous Zn scaffolds for biomedical applications, Mater. Des. 108 (2016) 136– 144
- [35] S. Thomas, I.S. Cole, M. Sridhar, N. Birbilis, Revisiting zinc passivation in alkaline solutions, Electrochim. Acta. 97 (2013) 192–201.
- [36] S. Thomas, N. Birbilis, M.S. Venkatraman, I.S. Cole, Corrosion of Zinc as a Function of pH, Corros. Sci. Section. 68 (2012) 015009–1–015009–9.
- [37] Z.Y. Chen, D. Persson, C. Leygraf, Initial NaCl-particle induced atmospheric corrosion of zinc–Effect of CO₂ and SO₂, Corros. Sci. 50 (2008) 111–123.
- [38] H.T. Yang, X.H. Qu, W.J. Lin, D.F. Chen, D.H. Zhu, K.R. Dai, Y.F. Zheng, Enhanced osseointegration of Zn-Mg composites by tuning the release of Zn ions with sacrificial mg-rich anode design, ACS Biomater. Sci. Eng. 5 (2018) 453–467.
- [39] H.B. Gong, K. Wang, R. Strich, J.G. Zhou, In vitro biodegradation behavior, mechanical properties, and cytotoxicity of biodegradable Zn-Mg alloy, J. Biomed. Mater. Res. Part B. 103 (2015) 1632–1640.
- [40] S. Champagne, E. Mostaed, F. Safizadeh, E. Ghali, M. Vedani, H. Hermawan, In vitro degradation of absorbable zinc alloys in artificial urine, Materials 12 (2019) 295–308.
- [41] K. Patai, M. Berenyi, M. Sipos, B. Noszal, Characterization of calcified deposits on contraceptive intrauterine devices, Contraception 58 (1998) 305–308.
- [42] T. Prosek, A. Nazarov, U. Bexell, D. Thierry, J. Serak, Corrosion mechanism of model zinc-magnesium alloys in atmospheric conditions, Corros. Sci. 50 (2008) 2216–2231.
- [43] G.K. Levy, J. Goldman, E. Aghion, The prospects of zinc as a structural material for biodegradable implants—a review paper, Metals 10 (2017) 1–18.

- [44] S.M. Zhu, C.C. Wu, G.N. Li, Y.F. Zheng, J.F. Nie, Microstructure, mechanical properties and creep behaviour of extruded Zn-xLi (x = 0.1, 0.3 and 0.4) alloys for biodegradable vascular, Mater. Sci. Eng. A. 10 (2020) 139082.1–139082.7.
 [45] N. Eliaz, Corrosion of metallic biomaterials: a review, Mater 12 (2019) 1–92.
 [46] M. Traisnel, D.L. Maguer, H.F. Hildebrand, A. lost, Corrosion of surgical implants, Clin. Mater. 5 (1990) 309–318.

- [47] J.E. Schaffer, E.A. Nauman, L.A. Stanciu, Cold drawn bioabsorbable ferrous and ferrous composite wires: an evaluation of *in vitro* vascular cytocompatibility, Acta Biomater. 9 (2013) 8574–8584.
- [48] L.G. Feo, The pH of the human uterine cavity *in situ*, Am. J. Obstet. Gynecol. 70 (1955) 60–64.